Design parameters effects on relative density of triply periodic minimal surfaces for additive manufacturing

E.A. Ramírez, Nicolas Béraud, Franck Pourroy, François Villeneuve, Matthieu Museau

Available online at www.sciencedirect.com

ScienceDirect

Procedia CIRP 00 (2019) 000–000

www.elsevier.com/locate/procedia

31st CIRP Design Conference 2021 (CIRP Design 2021)

Design parameters effects on relative density of triply periodic minimal surfaces for additive manufacturing

E. A. Ramírez[a,*], N. Béraud[a], F. Pourroy[a], F. Villeneuve[a], M. Museau[a]

[a]*Univ. Grenoble Alpes, CNRS, Grenoble INP, G-SCOP, 38000 Grenoble, France*

* Corresponding author. Tel.: +33-(0)74-904-0371. *E-mail address:* emilio-adrian.ramirez-salazar@grenoble-inp.fr

Abstract

Three-dimensional patterns have been widely considered for the generation of lightweight internal structures in design methodologies for additive manufacturing. Accordingly, triply periodic minimal surfaces patterns have been previously explored due to their improved mechanical performance compared to traditional lattice structures. The present study analyses the effect of the design parameters on relative density of Primitive and Gyroid patterns. Results show a linear correlation between the relative density and pattern's thickness, and a non-linear relationship to length. Relative density equations are proposed to ultimately aid in the pattern's dimensions selection based on manufacturing constraints for their applicability in topological optimization procedures.

Keywords: Geometric modelling; design method; additive manufacturing, triply periodic minimal surface.

1. Introduction

Additive manufacturing (AM) is a novel fabrication technology that has presented promising advantages over traditional manufacturing processes regarding its ability to directly produce functional parts of increasing complexity and topology [1,2]. To take advantage of the AM potential, design for additive manufacturing (DFAM) methodologies have been established to include topology optimization strategies and design for multi-scale structures, among other considerations [3]. In particular, topological design mindset aims to configure the structural part to carry loads at lowest weight, while permitting the intervening space to spatially distribute plastic deformations in energy absorption scenarios, among other functionalities [4].

Accordingly, cellular materials, constructed by a connected network of individual base cells, can be arranged to create strong load-bearing structures [5], and their capability of simultaneous optimization of stiffness, strength and weight have been considered attractive in the development of lightweight structures from topological strategies [3].

Recent studies have focused in the implementation of Triply periodic minimal surfaces (TPMS) for layer infill generation [6], which are a special kind of mathematically-defined zero-mean curvature surfaces. One of the benefits of this type of structures is the possibility to create materials with continuous and interconnected reinforcements, given their capacity to divide space into continuous phases [7]. Moreover, they have been deemed suitable as an alternative for lightweight structures development, due to their overall better mechanical performance compared to common computer-aided design (CAD) lattices [8].

Particularly, TPMS modelled body-centered cube (BCC) lattices with volume fractions between 10% and 30% have shown an increase of the elastic modulus, yield strength and compression strength compared to CAD generated alternatives [9]. Furthermore, a comparison between the energy absorption of BCC lattices and Primitive, Diamond and Gyroid patterns, which are common examples of TPMS structures, has shown that Diamond patterns have an overall highest mechanical performance, followed by Gyroid, Primitive patterns and BCC lattices [10].

Nomenclature

α	Constant factor for linear dependency
β	Constant factor for power dependency
C	Level set parameter
$f_{P,G}$	TPMS shape function
d	Pattern thickness
γ_k	Gradient step value
$\boldsymbol{\theta}_k$	Optimization vector
L	Unit-cell length
L_i	Pattern length
λ_i	Dilatation factor
n_i	Number of unit-cell instances
RD	Relative density from CAD data
ρ^*	Relative density function
RSS	Residual Sum of Squares

Regarding TPMS geometric characterization, previous studies have tested the effects of variating a level set parameter included in mathematical definition of the TPMS surfaces, which determines the volume fractions pertaining to the regions separated by the surface [11], and is used to control the position of the boundary between void and solid material [9]. The variation of the level set parameter in Gyroid patterns was tested, concluding that the relative density, or the ratio between the pattern volume and the bounding box volume, is directly proportional to the values of the level set parameter [11].

However, models obtained directly by this approach do not maintain a constant distribution of thickness along the pattern's unit-cells, which can present heat dissipation issues in metallic AM process such as Selective laser melting (SLM), or path programming control in Wire and arc additive manufacturing (WAAM); aside from the complexity of correlating the relative density of the structures to measurable thicknesses and lengths.

Further studies have developed constant thickness models by offsetting the TPMS fundamental shape in mechanical characterization tests [7,8,10], but there is no information available for the effects of the thickness and length in the relative density of the patterns. Ultimately, the use of this information is of great importance to aid in the pattern's dimensions selection, accounting for AM process constraints, for their applicability in topological optimization procedures, specifically in their utilization in solid isotropic material with penalization (SIMP) algorithm of intermediate densities. The use of variable density entities has been previously identified as an opportunity to further improve this approach of topological optimization [12].

Therefore, the main objective of the present study is to explore the design parameters effects, *i.e.* the thickness d and the unit-cell length $L = L_i/n_i$, defined as the size of each individual pattern instance, in the relative density of constant thickness Primitive and Gyroid TPMS patterns. The considered design parameters are depicted in Fig. 1.

The manufacture of TPMS structures have been previously studied for SLM [6,8–10], Selective laser sintering (SLS) [7], and stereolithography (SLA) [3,11], among other technologies, however, there is no information in the current literature for their fabrication in WAAM.

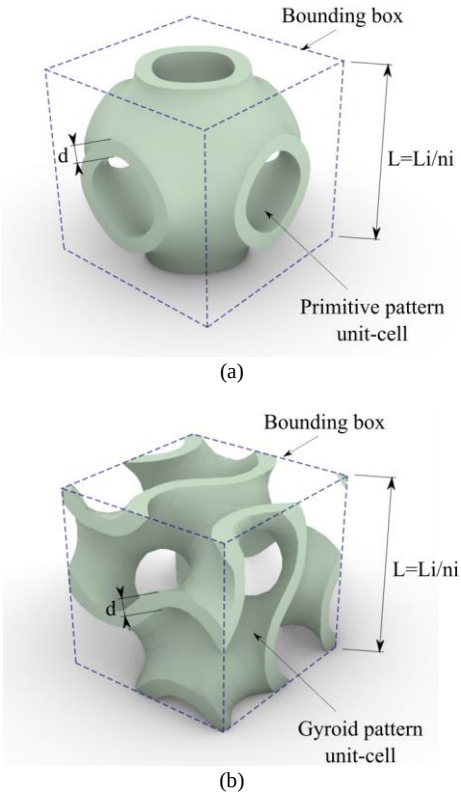

Fig. 1. Design parameters for a) Primitive and b) Gyroid TPMS patterns.

In the context of this study, future work aims to test the manufacturability of these structures by WAAM processes, therefore, the dimensions used for the modelling stages were selected according to previously defined manufacturing constraints.

The organization of the present document is as follows: initially the mathematical definition of the studied patterns is detailed, as well as the design methodology used to develop TPMS models. With the described methodology, several sets of Primitive and Gyroid models are generated.

The relative density obtained from CAD data is then correlated to the design parameters to analyse their effects and develop relationship equations for each studied pattern. Subsequently, the relative density equations are fine-tuned to minimize approximation errors. Maximum percentual error and Residual Sum of Squares results for before and after the function parameter's optimization procedures are finally presented before concluding on this study.

2. TPMS pattern modelling

This section initially details the mathematical definitions for Primitive and Gyroid patterns, and the main algorithm considered for surface generation. Lastly, the general TPMS design methodology used for the models' construction is detailed.

2.1. TPMS surface generation

Regarding TPMS's generation, surface's shape is controlled by pattern-specific implicit equations. For the purpose of this

study, the functions f_P for Primitive and f_G for Gyroid surfaces are detailed in Eq. 1 and Eq. 2, respectively; and were adapted from a review on general algorithms and equations for TPMS geometries by von Schnering and Nesper [13] and a combination of previous efforts presented in the literature [3,6,9–11]. From the equations, the patterns' periodicity is controlled by the dilatation factor λ_i, as a function of the number n_i of unit-cell instances in a three-dimensional pattern assembly and the size L_i of these instances in the x, y and z directions, as shown on Eq. 3.

$$f_P(x,y,z) = \cos(\lambda_x x) + \cos(\lambda_y y) + \cos(\lambda_z z) \quad (1)$$

$$f_G(x,y,z) = \cos(\lambda_x x)\sin(\lambda_y y) + \cos(\lambda_y y)\sin(\lambda_z z) + \cos(\lambda_z z)\sin(\lambda_x x) \quad (2)$$

$$\lambda_i = 2\pi \frac{n_i}{L_i}, \text{ for } i = x,y,z \quad (3)$$

For the surface representation, TPMS modelling commonly utilises the Marching Cubes algorithm, which is a common effective procedure to extract iso-surfaces in 3D-data fields [6]. The algorithm generates the surface in a cubic voxelization approach by evaluating the implicit function $v(x,y,z)$, presented in Eq. 4. Each voxel is defined to contain or be outside of the surface, hence, regions where $v(x,y,z) \leq 0$ are defined to have a portion of the surface, while regions where $v(x,y,z) > 0$ are defined as voids. From Eq. 4, a set value of $C = 0$ in the Marching Cubes algorithm is used to generate the TPMS fundamental shape.

$$v(x,y,z) = f_{P,G}(x,y,z) - C \quad (4)$$

2.2. General TPMS modelling methodology

The modelling methodology used to obtain the TPMS patterns is shown on Fig. 2, which was implemented in Rhinoceros 6 CAD Suite, utilising the Grasshopper graphical programming tool for the surface parametric definition and the Millipede extension for the main surface shape generation.

The general modelling starts with the input's definition, namely the pattern length L_i and thickness d, and the number of instances n_i required in a pattern matrix assembly. Subsequently, the TPMS function evaluation initially considers both L_i and n_i to define the pattern periodicity and the function domain to construct the mathematical identity of the desired pattern, which is stored in a function component.

This function component is then followed by an Iso-surface tool that performs the Marching cubes algorithm that generates the fundamental shape of the pattern. The resulting shape is then used as a central surface from which the inner and outer boundaries of the final model are obtained by offsetting half the desired pattern thickness d in both directions.

Final mesh operations consider the trimming and closing operations of the boundary mesh in the external unit-cell faces to define a closed structure.

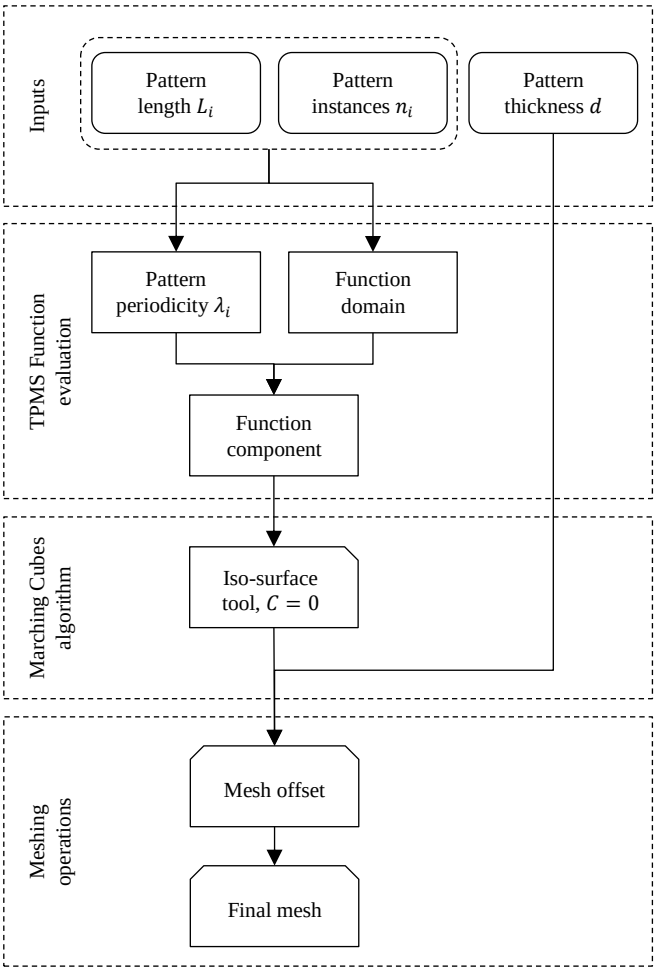

Fig. 2. TPMS pattern's modelling methodology.

3. Pattern design parameters' relationship analysis

Following the proposed modelling procedure, several models sets with diverse lengths and thicknesses were generated for Primitive and Gyroid patterns. All data in the next sections corresponds to single pattern models (one unit-cell) values, as they presented negligible relative density variance from pattern matrix assembly's data (percentual differences below 0.07%), and better modelling computing performance.

In addition, models where developed to be contained in a cubic bounding box of size L (as shown on Fig. 1), complying with a condition of $\lambda_x = \lambda_y = \lambda_z$. For each model, the relative density RD from the CAD data was calculated as the ratio between the pattern volume and the cubic bounding box, as shown on Eq. 5.

$$RD = \frac{pattern\ volume}{bounding\ box\ volume} \quad (5)$$

The next subsections present in detail the model's dimensions used for testing, the graphical representation of the obtained data and the relative density function development.

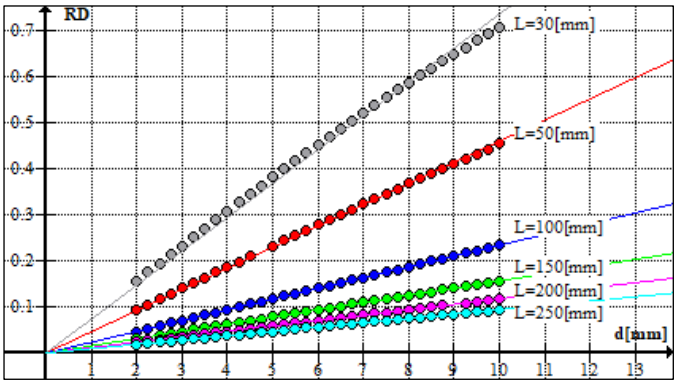

Fig. 3. Relative density RD as a function of thickness d in constant-thickness Primitive unit-cells.

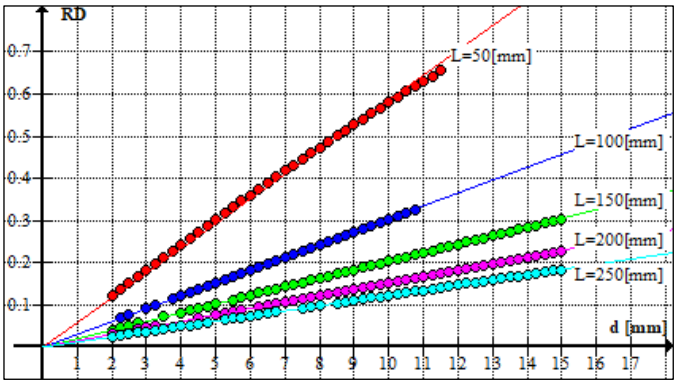

Fig. 5. Relative density RD as a function of thickness d in constant-thickness Gyroid unit-cells.

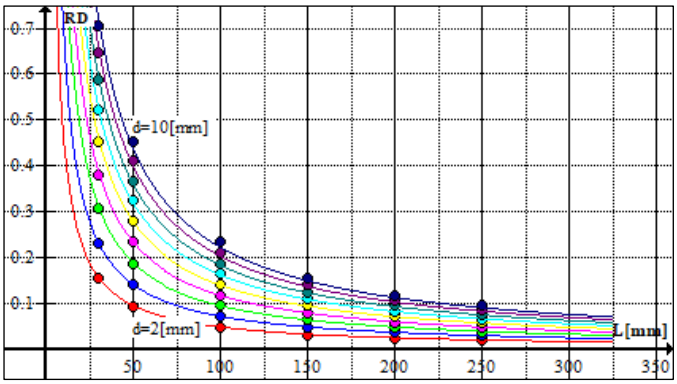

Fig. 4. Relative density RD as a function of length L in constant-thickness Primitive unit-cells.

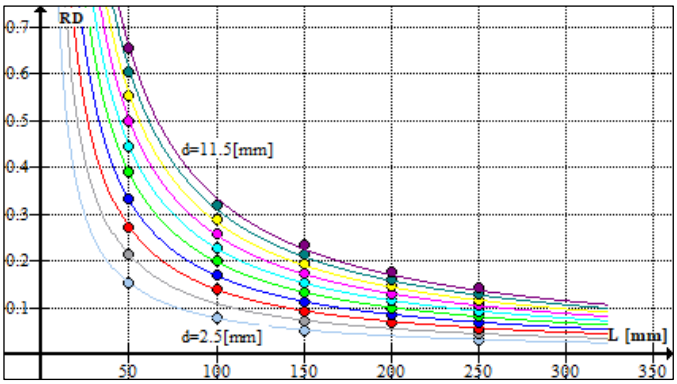

Fig. 6. Relative density RD as a function of length L in constant-thickness Gyroid unit-cells.

3.1. Primitive patterns

Primitive unit-cell models with lengths between 30 and 250mm, and thicknesses between 2 and 10mm were considered for the analysis of the effect of design parameters on the relative density.

The dependency of the relative density with the pattern thickness d was initially explored by plotting the diverse RD values obtained for each model. As shown on Fig. 3, there is a linear relationship between the relative density and d, and the slope tends to decay for larger values of L.

Afterwards, a relative density *vs* L graph, shown on Fig. 4, was used to explore the effects of L variation, which exhibits a non-linear decreasing dependence. From Fig. 4, the curves correspond to the different values of d, with 1mm increments. Only labels for 2 and 10mm were added due to visualization restrictions.

3.2. Gyroid patterns

The same detailed procedure was used to generate Gyroid patterns models with lengths between 50 and 250mm, and thicknesses between 2 and 15mm.

As evidenced by Fig. 5 and Fig. 6, Gyroid patterns present the same behaviour as in Primitive patterns regarding the relationships of RD with d and L, respectively. Similarly, Fig 6 only presents labels for 2.5 and 11.5mm due to visualization restrictions. Each curve represents an increment of 1mm in thickness.

Even though the models generated for thicknesses between 2 and 15mm were considered to the initial dependency verification regarding d, the study of the relationships with respect to L and the subsequent analysis for function development in Gyroid patterns considers the models between 2.5 and 11.5mm, for a more uniform data point distribution.

3.3. Relative density function development

In an effort to develop a general equation for relative density as a function of both pattern's thickness d and length L, Eq. 6 shows the proposed model which combines the linear relationship with d and a decreasing power relationship regarding L; α and β are considered as constants.

$$\rho^*(d, L) = \alpha\, d\, L^{-\beta} \tag{6}$$

Initial power curve fitting was employed to estimate the curve's exponents variation in the data plotted on the RD vs L graphs (Fig. 4 and Fig 6). Even though the proposed model considers d and L to be independent, a slight linear correlation was found between the β exponent value and d. Nevertheless, this exponent was treated as a constant equal to the mean value of the obtained exponents. Accordingly, the resulting constant factors for power dependency obtained were $\beta_P = 0.981$ and $\beta_G = 0.978$ for Primitive and Gyroid patterns, respectively.

This particular assumption was further verified by fitting the data points to a curve of the form $\rho_P^*(L) = \alpha\, d\, L^{-0.981}$ for

Primitive patterns, and $\rho_G^*(L) = \alpha\, d\, L^{-0.978}$ for Gyroid patterns, and evidenced by a resulting R^2 value between 0.99 and 1. Subsequently, the constant factors for lineal dependency $\alpha_P = 2.081$ and $\alpha_G = 2.607$ were determined for Primitive and Gyroid patterns, respectively.

4. Relative density function's factors optimization

With the initial values obtained for α and β, the relative density of the models was calculated and compared to the initial RD data, resulting in an overall absolute percentual error between 0.97% and 4.51% in Primitive patterns, and between 0.22% and 7.72% for Gyroid patterns. To correct these deviations, a Gradient Descent optimization algorithm was employed to reduce the Residual Sum of Squares, defined by Eq. 7, where j corresponds to the different sets of (d, L).

$$RSS(\alpha, \beta) = \sum_j \left(\rho^*(d, L)_j - RD_j\right)^2 \quad (7)$$

The Gradient Descent optimization procedure is detailed on Appendix 1. In this process, the CAD data is initially stored in a RD variable. Later, the RSS function is constructed and the values found for α and β are considered as an initial guess $\boldsymbol{\theta}_0(\alpha_0, \beta_0)$ and stored in a separate variable $\boldsymbol{\theta}_k$ to be used in the iterative process.

In each iteration, a new value $\boldsymbol{\theta}_{k+1}$ is calculated as a decrease of $\gamma_k \nabla RSS(\boldsymbol{\theta}_k)$ from an initial $\boldsymbol{\theta}_k$, where γ_k is the step value and $\nabla RSS(\boldsymbol{\theta}_k)$ is the gradient of RSS evaluated at $\boldsymbol{\theta}_k$. The algorithm ends once the variation of $\gamma_{k+1} - \gamma_k$ falls below a precision value, which was fixed at 1E-06.

4.1. Primitive patterns: ρ_P^* function optimization results

With the initial guess of $(\alpha_0, \beta_0) = (2.081, 0.981)$, a Python script running the detailed algorithm was developed to obtain the optimized parameters $(\alpha, \beta) = (2.141, 0.982)$ after 20 iterations, using an initial step value $\gamma_0 = 0.001$. The corrected equation $\rho_P^*(d, L)$ for Primitive patterns is shown on Eq. 8.

$$\rho_P^*(d, L) = 2.141\, d\, L^{-0.982} \quad (8)$$

Table 1 summarizes the RSS and the absolute percentual error results before and after the Gradient Descent optimization. In general, the maximum absolute percentual error dropped from 4.51% to 1.98% for L values between 50 and 250mm, with a one order of magnitude reduction of the obtained RSS.

Percentual error and RSS data are also presented for each tested length. Equation errors tends to decrease as the length increases. As illustrated by the graphical data, the models considered for larger lengths correspond to lower relative density scenarios, which are better adjusted to the linear tendency regarding d. From Fig. 3, this linear dependency tends to decay for relative densities of above 0.6, mainly evidenced in the data for L =30mm (Fig. 3).

Table 1. RSS and absolute percentual error differences before and after Gradient Descent optimization in equation parameters for Primitive patterns.

L [mm]	Initial		After Gradient Descent	
	RSS	Max. error %	RSS	Max. error %
Overall	2.57E-03	4.51	2.85E-04	1.98
L=50[mm]	1.76E-03	4.51	2.59E-04	1.98
L=100[mm]	5.51E-04	3.30	1.36E-05	0.87
L=150[mm]	1.72E-04	2.56	4.34E-07	0.20
L=200[mm]	6.09E-05	2.01	3.62E-06	0.53
L=250[mm]	2.68E-05	1.59	7.69E-06	0.84

Table 2. RSS and absolute percentual error differences before and after Gradient Descent optimization in equation parameters for Gyroid patterns.

L [mm]	Initial		After Gradient Descent	
	RSS	Max. error %	RSS	Max. error %
Overall	2.16E-02	7.72	3.28E-03	4.34
L=50[mm]	9.72E-03	7.72	2.83E-03	4.34
L=100[mm]	4.45E-03	6.60	3.50E-04	2.40
L=150[mm]	4.17E-03	5.79	4.14E-05	1.13
L=200[mm]	2.10E-03	5.17	1.25E-05	0.57
L=250[mm]	1.19E-03	4.72	4.53E-05	0.99

Although model data for lengths of 30mm were used to develop the initial guess (α_0, β_0), their corresponding RD data were not used to calculate the optimized parameters, as they introduced errors due to their non-linear behaviour in larger relative density values. A different scenario of initial guess estimation considering this data was also tested, resulting in the same optimized parameters after a longer iterative process, however, their data is not reported in this document.

4.2. Gyroid patterns: ρ_G^* function optimization results

With an initial guess of $(\alpha_0, \beta_0) = (2.607, 0.978)$, the optimized parameters $(\alpha, \beta) = (2.568, 0.966)$ were obtained after 10 iterations using an initial step value $\gamma_0 = 0.001$. The corrected equation $\rho_G^*(d, L)$ for Gyroid patterns is shown on Eq. 9.

$$\rho_G^*(d, L) = 2.568\, d\, L^{-0.966} \quad (9)$$

Table 2 summarizes the RSS and the absolute percentual error results before and after the Gradient Descent optimization for constant thickness Gyroid patterns. There is an overall reduction of the maximum absolute error from 7.72% to 4.34%, and a decrease of one order of magnitude for the overall RSS. Similarly, the same effect of error increase for smaller lengths (larger relative density scenarios) was found for Gyroid patterns. In addition, Gyroid patterns tends to present a bigger relative density than Primitive models for a set value of thickness and/or length, hence the increase in the reported RSS and maximum percentual errors.

5. Conclusions

In the present study, a general modelling methodology based on the offsetting of TPMS obtained by a Marching cubes algorithm was used to develop different sets of Primitive and Gyroid patterns, to study the effects on relative density of the pattern's thickness d and unit-cell length L. As stated before, no information was found in the available literature regarding the combined effect of thickness and length on the relative density of Primitive and Gyroid patterns. This present study fills this gap in geometric modelling analysis and ultimately proposes tools for the calculation of relative density.

Preliminary observations showed that the relative density of the models present a linear relationship with respect to d and a decreasing power relationship regarding L. Specifically, the linear dependency is particularly beneficial for the implementation of density-graded structures. Gyroid patterns tends to present bigger relative density than Primitive models for a set value of thickness and/or length

Furthermore, equations for the pattern's relative density as a function of both thickness and length were proposed. The percentual error between the relative density obtained from CAD data and the values obtained from the equations were calculated, having a maximum of 4.51% in Primitive patterns, and 7.72% for Gyroid patterns. Even though percentual errors results for Gyroid models were greater than the values found in Primitive models, they are due to the bigger relative density scenarios studied, as it is found that for these cases the linear dependency with respect to the thickness start to decay. The main applicability of the studied TPMS is considered for lightweight structures, thus this non-linearity is acknowledged but not further corrected. In an effort to reduce the maximum reported errors, a Gradient Descent optimization procedure was used to fine-tune the factors for linear and power dependency and reduce the function Residual Sum of Squares. Using this procedure, corrected equations are proposed, which presented a reduction of the maximum percentual errors to 1.98% in Primitive patterns and 4.34% for Gyroid patterns. RSS were reduced in one order of magnitude for both studied surfaces.

Future work is aimed to the development of varying density TPMS models by Wire and arc additive manufacturing (WAAM) process, and the application of the proposed equations to aid in the development of density graded structures resulting from topological optimization procedures, while considering manufacturing constraints for the definition of the required lengths and thicknesses.

Acknowledgements

This work is supported by the ANR BeShape project, of the French Agence Nationale de la Recherche, Paris, France [grant number ANR-18-CE10-0014-01]

Appendix A. Algorithm for equation factor's optimization

Algorithm 1 details the procedure followed for the linear and power factor optimization for the reduction of the Residual Sum of Squares of the proposed equations.

Algorithm 1. Gradient Descent for (α, β) optimization

1. $RD \leftarrow$ Rhinoceros data
2. Construct $RSS(\alpha, \beta)$
3. $\boldsymbol{\theta}_0 \leftarrow \alpha_0, \beta_0$
4. $\boldsymbol{\theta}_k \leftarrow \theta_0$
5. Repeat
   a. $\boldsymbol{\theta}_{k+1} = \boldsymbol{\theta}_k - \gamma_n \nabla RSS(\boldsymbol{\theta}_k)$
   b. γ_{n+1} adjustment
   c. if $RSS(\boldsymbol{\theta}_{k+1}) < RSS(\boldsymbol{\theta}_k)$, then $\boldsymbol{\theta}_k \leftarrow \boldsymbol{\theta}_{k+1}$
6. Until $\gamma_{k+1} - \gamma_k < precision$
7. Return $\boldsymbol{\theta}_{k+1}$

References

[1] W. Gao et al. The status, challenges, and future of additive manufacturing in engineering. Computer-Aided Design; 2015; vol. 69, p. 65–89.

[2] B. Vayre, F. Vignat, and F. Villeneuve. Metallic additive manufacturing: state-of-the-art review and prospects. Mechanics & Industry; 2012; vol. 13, no. 2, p. 89–96.

[3] D. Li, W. Liao, N. Dai, G. Dong, Y. Tang, and Y. M. Xie. Optimal design and modeling of gyroid-based functionally graded cellular structures for additive manufacturing. Computer-Aided Design; 2018; vol. 104, p. 87–99.

[4] A. G. Evans, J. W. Hutchinson, N. A. Fleck, M. F. Ashby, and H. N. G. Wadley. The topological design of multifunctional cellular metals. Progress in Materials Science; 2001; vol. 46, no. 3, p. 309–327.

[5] M. F. Ashby. The properties of foams and lattices. Philosophical Transactions of the Royal Society A: Mathematical, Physical and Engineering Sciences; 2006; vol. 364, no. 1838, p. 15–30.

[6] J. Feng, J. Fu, Z. Lin, C. Shang, and X. Niu. Layered infill area generation from triply periodic minimal surfaces for additive manufacturing. Computer-Aided Design; 2019; vol. 107, p. 50–63.

[7] D. W. Abueidda, M. Elhebeary, C.-S. (Andrew) Shiang, S. Pang, R. K. Abu Al-Rub, and I. M. Jasiuk. Mechanical properties of 3D printed polymeric Gyroid cellular structures: Experimental and finite element study. Materials & Design; 2019; vol. 165, p. 107597.

[8] F. S. L. Bobbert et al. Additively manufactured metallic porous biomaterials based on minimal surfaces: A unique combination of topological, mechanical, and mass transport properties. Acta Biomaterialia; 2017; vol. 53, p. 572–584.

[9] M. Zhao, F. Liu, G. Fu, D. Z. Zhang, T. Zhang, and H. Zhou. Improved Mechanical Properties and Energy Absorption of BCC Lattice Structures with Triply Periodic Minimal Surfaces Fabricated by SLM. Materials; 2018; vol. 11, no. 12, p. 2411.

[10] L. Zhang et al. Energy absorption characteristics of metallic triply periodic minimal surface sheet structures under compressive loading. Additive Manufacturing; 2018; vol. 23, p. 505–515.

[11] D. Li, W. Liao, N. Dai, and Y. M. Xie. Comparison of Mechanical Properties and Energy Absorption of Sheet-Based and Strut-Based Gyroid Cellular Structures with Graded Densities. Materials; 2019; vol. 12, no. 13, p. 2183.

[12] D. Brackett, I. Ashcroft, and R. Hague. Topology Optimization for Additive Manufacturing. Proceedings of the 2011 International Solid Freeform Fabrication Symposium; 2011; p. 15.

[13] H. G. von Schnering and R. Nesper. Nodal surfaces of Fourier series: Fundamental invariants of structured matter. Z. Physik B - Condensed Matter; 1991; vol. 83, no. 3, p. 407–412.